Surfaces, Interfaces, and Catalysis; Physical Properties of Nanomaterials and Materials

Spontaneous Formation of >90% Optically Transmissive, Electrochemically Active CoP Films for Photoelectrochemical Hydrogen Evolution

Paul Andrew Kempler, Harold J. Fu, Zachary P. Ifkovits, Kimberly M. Papadantonakis, and Nathan S. Lewis

Just Accepted

Spontaneous Formation of >90% Optically Transmissive, Electrochemically Active CoP Films for Photoelectrochemical Hydrogen Evolution

Paul A. Kempler[1], Harold J. Fu[1], Zachary P. Ifkovits,[1] Kimberly M. Papadantonakis[1], Nathan S. Lewis[1,2]*

[1]Division of Chemistry and Chemical Engineering, California Institute of Technology, Pasadena, CA 91125
[2]Beckman Institute, California Institute of Technology, Pasadena, CA 91125

*Corresponding Author: nslewis@caltech.edu

Abstract

Earth-abundant catalysts for the hydrogen-evolution reaction require increased mass loadings, relative to Pt films, to achieve comparable activity and stability in acidic electrolytes. We report herein that spontaneous nanostructuring of opaque, electrodeposited CoP films, 40-120 nm in thickness, leads to transparent electrocatalyst films that exhibit up to 90% optical transmission in the visible spectrum. The photocurrent density under simulated sunlight at a representative n^+p-Si(100)/CoP photocathode increases by 200% after exposure to 0.50 M H_2SO_4(aq) and remains stable for 12 h of continuous operation. Atomic-force microscopy and scanning-electron microscopy of the film before and after exposure to 0.50 M H_2SO_4(aq) validate an optical model for transparent CoP films as probed with spectroscopic ellipsometry.

TOC graphic
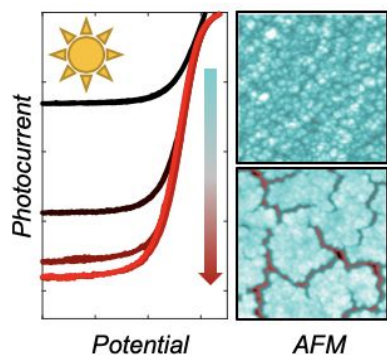
KEYWORDS Photoelectrochemistry, Solar Fuels, Catalysts, Photocathode, Phosphides

Integration of semiconductors with catalysts for the hydrogen-evolution reaction (HER) is an important step in the construction of fully integrated devices for the photoelectrochemical conversion of water and sunlight into fuel.[1-2] Deposition of metallic catalysts onto the light-absorbing surface of semiconductors typically results in parasitic reflection and absorption of light, resulting in a tradeoff between increases in optical losses and decreases in overpotential for the HER.[3-4] This tradeoff is especially important when earth-abundant HER catalysts are used in photoelectrochemical devices, because increased loadings of such electrocatalysts are typically required, relative to Pt, to reach equivalent rates of reaction.[5-6] Backside illumination of silicon photocathodes, in which the Pt electrocatalyst films are opposite the light-absorbing face of the semiconductor, has led to electrodes that exhibit photocurrents which are insensitive to the catalyst loading.[7-9] Textured Si surfaces minimize reflection losses and have been integrated with films <10 nm in thickness of metal phosphide HER catalysts to achieve absolute photocurrent densities >35 mA cm^{-2}.[10-11] Microstructured semiconductors, such as Si microwires, have been used to spatially separate surfaces used for light absorption from surfaces loaded with opaque films of NiMo and CoP HER electrocatalysts.[12-15] Microstructuring strategies are limited to semiconductors with long carrier diffusion lengths and lead to a loss in photovoltage due to increased area available for carrier recombination. Transparent metal films could allow for uniform catalyst coverage on the light-absorbing surface of planar, textured, or microstructured semiconductors, which would facilitate integration in a wide range of potential solar-to-fuel device configurations. Such an approach could be used alone or in tandem with other light management strategies, such as the patterning of metal electrocatalyst islands.[16-17]

Semiconducting transition-metal selenides and transition-metal sulfides, which require absolute overpotentials of 150-183 mV to drive the HER at a rate corresponding to a current

density (J) of -10 mA cm^{-2}, have been integrated with textured, antireflective silicon photocathodes as uniform, amorphous films, approximately 50 nm in thickness. Such devices have exhibited high photocurrent densities ($|J| > 30$ mA cm^{-2}) for 2 h in 0.50 M H_2SO_4(aq).[18-20] Substantially longer stabilities under reductive bias, and thus increased catalyst loadings or more stable catalyst materials, are required for a practical solar-to-fuels device. Transparent metal films with an open micro- or nano-structure have been prepared from precious metals such as Pt, Pd, Re, and Rh by controlled deposition or by etching in acidic electrolytes. Such Pt and Rh films have been integrated as catalysts into efficient and stable devices for photoelectrochemical hydrogen evolution.[21-23] Pt films on p-InP photocathodes have been reported to exhibit substantial optical transparency for 20 h in 4.0 M $HClO_4$(aq).[24]

The optical properties of nanostructured metal films are strong functions of the volume fraction and orientation of voids within the film, but are relatively insensitive to the nature of the host metal.[25] Hence, similar optical properties should be observable in films composed of a wide range of metals and HER electrocatalysts, including transition-metal phosphides, a class of materials that is capable of driving HER current densities of -10 mA cm^{-2} at absolute overpotentials < 100 mV in acidic media.[26-28] Within the family of transition-metal phosphides, CoP exhibits one of the highest average turnover frequencies per surface site, due to its intermediate binding energy for molecular hydrogen.[5] High-surface-area, amorphous CoP films can be prepared at room temperature and atmospheric pressure via electrodeposition from baths containing $CoCl_2$ and H_2PO_2 salts, with the deposited film containing oxidized cobalt and phosphorous species that are converted under cathodic bias in acidic media to a material with near-zerovalent Co and reduced P.[29-30] Prior reports of integration of electrodeposited CoP films

on planar p-Si and Cu$_2$O have focused on thick, discontinuous catalyst films whose performance are limited by a trade-off between optical losses and overpotential towards the HER.[13, 31]

We report herein a method for preparing transparent CoP films on Si(100) and fluorine-doped tin oxide (FTO) substrates. The electrocatalytic and optical properties of the films were assessed via optical transmission measurements during continuous hydrogen evolution in 0.50 M H$_2$SO$_4$(aq) to approximate conditions relevant to a solar-to-hydrogen device. A two-parameter optical model for the transparent, electrocatalytic CoP films was developed using spectroscopic ellipsometry, and the model was validated by independent measurements of the film nanostructure.
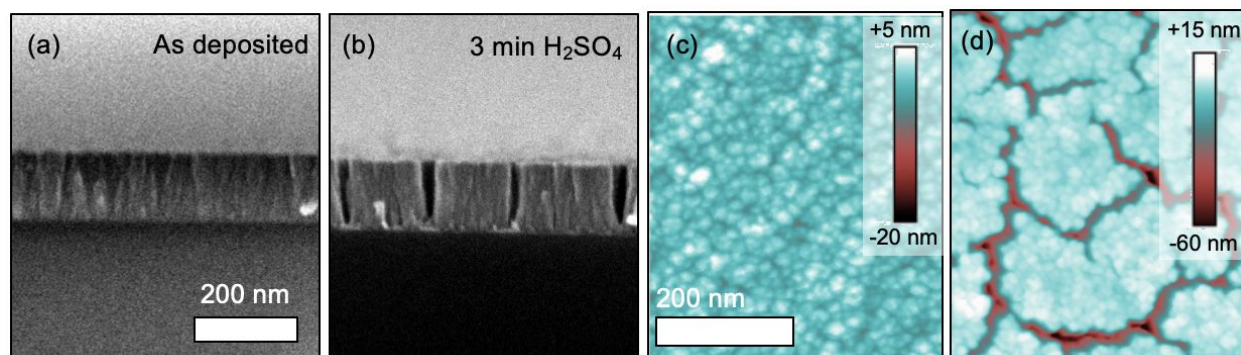
Figure 1

Figure 1: (a) SEM image of a cross section of a CoP film deposited onto n$^+$-Si(100)/Ti/Co and (b) exposed to 0.50 M H$_2$SO$_4$(aq) for 3 min. (c-d) AFM images of an as-deposited n$^+$-Si(100)/Ti/CoP surface recorded in tapping mode with a Si tip having a nominal radius of 2 nm and (d) after 3 min exposure to 0.50 M H$_2$SO$_4$(aq).

Figure 1a shows a representative SEM cross section of a CoP film that was electrodeposited onto n$^+$-Si to a loading of 1200 mC cm^{-2} (n$^+$-Si(100)/Ti/CoP(1200 mC cm^{-2})). Electrodeposition onto pre-nucleated, n$^+$-Si(100)/Ti/Co surfaces led to lustrous films with uniform coverage. Exposure of the films to 0.50 M H$_2$SO$_4$(aq) led to the dissolution of Co, which was accompanied by the formation of small H$_2$ bubbles on the surface. **Figure 1b** shows a

representative SEM cross section of the same film after 3 min of activation in 0.50 M H_2SO_4(aq).

Crevices that extended vertically from the surface to the substrate were observed, while the total

thickness of the film remaining essentially constant. Determination via inductively coupled

plasma mass spectrometry, ICP-MS, of the dissolution products of as deposited CoP films in

0.50 M H_2SO_4(aq) under cathodic bias, indicated that the majority of material removed was Co

(Figure S1). The majority of cobalt corrosion occurred within the first 10 min of exposure to 0.50

M H_2SO_4(aq) and the rate of corrosion continued to decrease from 1.5 to 0.12 ng s^{-1} cm^{-2} after 10

min and 6 hours of continuous cathodic bias, respectively (Figure S1c).

Figure 1c shows an AFM image of an electrodeposited CoP film on an n$^+$-Si(100)/Ti/Co

surface after 40 s of electrodeposition. The mean surface roughness was 1.2 nm and the surface

was composed of spherical grains that were 10-25 nm in diameter. Exposure of the film to 0.50

M H_2SO_4(aq) led to the formation of small crevices with a mean full width at half max (*FWHM*)

of 6 ± 3 and a depth (*d*) of 11 ± 3 nm after 1 min of immersion (Figure S2), with these values

increasing to *FWHM* = 13 ± 4 and *d* = 41 ± 15 nm after 3 min of exposure time (**Figure 1d**). The

formation of crevices led to a 50% increase in the nanoscale roughness, from 1.07 to 1.60 times

the geometric area of the film. The areal density of crevices, measured as the total length per unit

area, increased to 7.3 μm^{-1} after 60 s and remained essentially constant at 11.2 and 11.3 μm^{-1}

after 120 s and 180 s of exposure time, respectively. The rate of change in crevice height relative

to the rate of change in crevice width was 4 to 1.

Collective physical characterization indicates that the composition and structure of the as-

deposited film was suitable for spontaneous formation of nanostructured catalyst films having

feature sizes smaller than half the wavelength of visible light. Energy dispersive X-ray

spectroscopy,[13] X-ray photoelectron spectroscopy,[29] and X-ray absorption spectroscopy,[30] of

electrodeposited CoP have shown that that exposure of films to 0.50 M H_2SO_4(aq) leads to a reduction in the molar ratio of Co:P.[29-30] The predominance of Co in the corrosion products detected via ICP-MS is consistent with prior observations of a decrease in the Co:P ratio following acid exposure. During the first 10 minutes of exposure to electrolyte, phosphorus was detected as a minor product of corrosion, in insufficient amounts for quantification, and therefore phosphorus containing species are not the primary film components removed during activation.

Figure 2a shows a series of optical transmission spectra for a CoP film, as a function of time immersed in 0.50 M H_2SO_4(aq). The transmission of CoP films was characterized as a function of the applied electrochemical potential using transparent, conductive, FTO as a substrate. Immediately after immersion in 0.50 M H_2SO_4(aq), the films exhibited an optical transmittance ranging from 37% at 400 nm to 77% at 1000 nm. The weighted average transmittance, T_{avg}, was calculated from the individual fractional transmittance as a function of wavelength, weighted by the flux of photons at a given wavelength in the Air Mass (AM) 1.5 spectrum, and normalized to unity (Equation 1):

$$T_{avg} = \frac{1}{\int_{400}^{1100} \phi_{AM1.5}(\lambda)d\lambda} \int_{400 \text{ nm}}^{1100 \text{ nm}} \phi_{AM1.5}(\lambda)\, T(\lambda)\, d\lambda \tag{1}$$

$T(\lambda)$ represents the fractional transmittance and $\phi(\lambda)$ is the photon density per unit of wavelength in the solar spectrum. T_{avg} increased continuously with immersion time in the solution, from an initial value of T_{avg}= 0.67 to T_{avg}= 0.85 after 10 min at open circuit. Upon application of a cathodic current density of 10 mA cm^{-2}, relevant to photoelectrochemical H_2 evolution in unconcentrated sunlight, T_{avg} increased to 0.89 and remained stable for > 10 min of testing. At negative potentials for which cathodic current was observed, the transmittance increased by over 10% between λ = 400 and λ = 450 nm.

Irreversible changes in the optical properties of the CoP films correlated with the time scales observed for nanostructuring of the films. Application of a reducing bias produced improvements in the transmissivity that can be consistently ascribed to previously observed chemical changes in the film composition that occur under applied bias in 0.50 M H_2SO_4(aq), such as reduction of phosphorus and dissolution of cobalt oxide.[30]

Figure 2
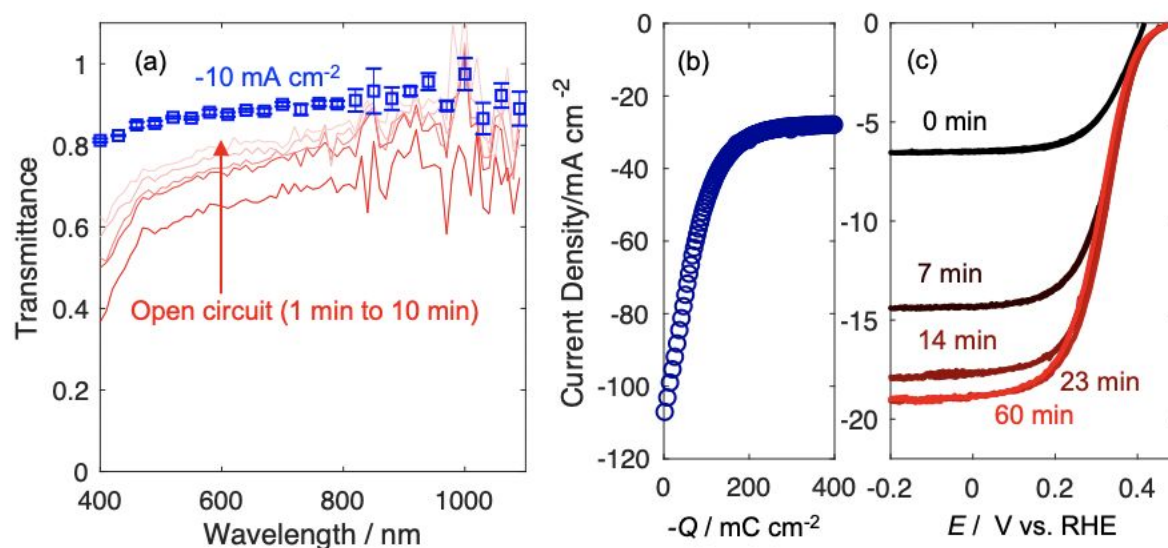
Figure 2: (a) In situ transmission versus wavelength measurements of a CoP film deposited to a charge density of 400 mC cm^{-2} onto an FTO/Co surface and immersed in 0.50 M H_2SO_4(aq). Red traces indicate transmission measurements collected sequentially at open circuit, while the blue data points represent the average transmission collected during 10 minutes of cathodic bias at -10 mA cm^{-2} (b) Photocurrent density vs. charge density, Q, passed for an n$^+$p-Si(100)/Ti/Co electrode during deposition of CoP at -0.60 V versus a saturated calomel electrode under high-intensity 625 nm illumination from a narrow-band light-emitting diode. (c) J-E behavior as a function of time for an n$^+$p-Si(100)/Ti/Co/CoP(400 mC cm^{-2}) electrode under 100 mW cm^{-2} of simulated Air Mass 1.5 illumination in 0.50 M H_2SO_4(aq) that was continuously purged with H_2(g). Scans were recorded at 50 mV s^{-1} and were separated by pauses at open circuit in the absence of illumination.

The optical properties of CoP were characterized on representative H_2-evolving photocathodes using metallized n$^+$p-Si(100)/Ti/Co samples as substrates. Crystalline Si exhibits long minority-carrier lifetimes, so the light-limited photocurrent density, J_{ph}, serves as a

quantitative measure of the total amount of photons that pass through the catalyst film and are collected by the Si. **Figure 2b** shows the effect of charge passed during CoP deposition, Q, on the photocurrent density of an n^+p-Si(100)/Ti/Co electrode. Deposition of 400 mC cm^{-2} of CoP at light-limited photocurrent densities led to a decrease in $|J_{ph}|$ from 107 mA cm^{-2} to 28 mA cm^{-2}. **Figure 2c** shows the current density vs potential (J-E) response of an n^+p-Si(100)/Ti/CoP(400 mC cm^{-2}) electrode, under 100 mW cm^{-2} of simulated AM1.5 illumination in H$_2$-saturated 0.50 M H$_2$SO$_4$(aq), as a function of the time spent in the acidic environment. Following pauses at open circuit in the absence of illumination, with successive scans -J_{ph} increased from 6.6 mA cm^{-2} to 19.1 mA cm^{-2}. For 12 h, the current density at 0.0 V versus the reversible hydrogen electrode (RHE) remained within 12% of the maximum value (Figure S3a). The potential at a n^+-Si(100)/Ti/CoP(800 mC cm^{-2}) in H$_2$-saturated 0.50 M H$_2$SO$_4$(aq), held at -10 mA cm^{-2} in the absence of direct illumination, was observed to gradually decrease relative to RHE (Figure S3b). Measurements of the optical properties of the CoP films in 0.50 M H$_2$SO$_4$(aq) showed that transmission of visible and infrared light through the film increased during the formation of crevices within the film, and conversion of the as-deposited species to metallic Co and reduced P at negative potentials led to further increases in the optical transmission.[30] The stability of photocurrents on a representative photocathode showed that the strategy of nanostructuring an otherwise opaque CoP film to achieve transmissivity does not necessarily lead to a substantial decrease in stability, because the stabilities of the electrodes observed herein were comparable to those reported previously for CoP in 0.50 M H$_2$SO$_4$(aq) (Table S1). The performance of the transparent catalyst films in this work was compared to the performance of nominally identical n^+p-Si(100)/Pt photocathodes (Figure S5).[14] The nanostructured CoP films in this work exhibited larger photocurrents than a n^+p-Si(100) photocathode decorated with a 4 nm thick sputtered Pt

film, indicating that the catalyst was more transmissive than the thin metal film despite being 10

times greater in thickness. However, the devices utilizing CoP as a catalyst reached a benchmark

current density of -10 mA cm^{-2} at potentials 150 mV more negative than the potentials required

for state-of-the-art n$^+$p-Si(100)/Pt photocathodes. Thus, the increased catalyst loading in the CoP

devices was not sufficient to offset the increased activity of Pt towards hydrogen evolution in

acid.

Figure 3
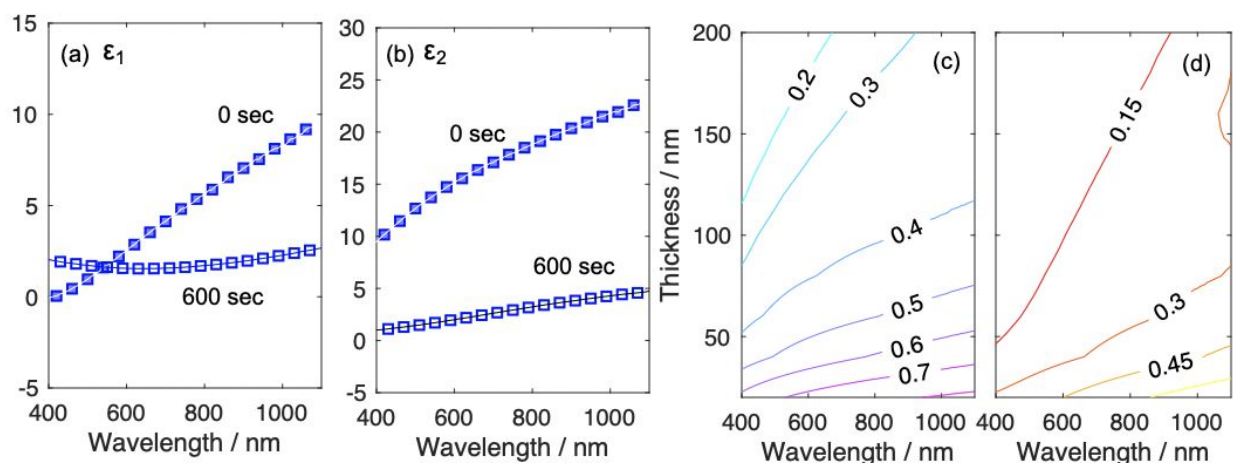
Figure 3: Spectroscopic ellipsometry of n$^+$-Si(100)/Ti/Co/CoP deposited to a charge density of 800 mC cm^{-2}. Measured data points are shown as individual markers, and fits are represented as continuous lines. (a) Real and (b) imaginary components of the dielectric functions of as deposited CoP films (filled markers) and films activated after 600 seconds of activation in 0.50 M H$_2$SO$_4$(aq) (open markers). (c) Modeled transmittance isolines as a function of film thickness for an EMA layer with void inclusions, f_m = 0.75, and q = 0.98. (d) Modeled transmittance isolines as a function of film thickness for an EMA layer with metal inclusions, f_m = 0.75, and q = 0.33.

The effects of the dielectric properties and nanostructure of CoP films on the

macroscopic optical properties were evaluated by use of spectroscopic ellipsometry. The

dielectric function, $\tilde{\varepsilon}$, is a complex function of wavelength that describes the average

macroscopic response resulting from the individually polarizable components of the film.[32]

Dielectric functions for the n$^+$-Si(100)/Ti/CoP samples were calculated from the measured

complex reflectance ratio using commercial software (WVASE®). The index of refraction, n, and extinction coefficient, k, of the as-deposited CoP films became increasingly insensitive to film thickness after >800 mC cm^{-2} of cathodic charge density had been passed. Relative to tabulated values for a Co film of comparable thickness,[33] the as-deposited CoP exhibited an increased n and decreased k from $\lambda = 400\text{-}1100$ nm (Figure S6). **Figure 3a** and **Figure 3b** present the real and imaginary components of $\tilde{\varepsilon}$, ε_1 and ε_2, respectively, for a CoP film deposited to a charge density of 800 mC cm^{-2} before and after exposure to 0.50 M H$_2$SO$_4$(aq). Measurements of the dielectric functions for catalyst films with variable thicknesses are presented in Figure S7.

The optical properties of electrodeposited CoP films before and after activation in 0.50 M H$_2$SO$_4$(aq) were modeled using a Maxwell-Garnett effective medium approximation,[34] (Equation 2)

$$\tilde{\varepsilon}_{eff} = \tilde{\varepsilon}_m + \frac{f_v(\tilde{\varepsilon}_v - \tilde{\varepsilon}_m)\tilde{\varepsilon}_m/[\tilde{\varepsilon}_m + q(\tilde{\varepsilon}_v - \tilde{\varepsilon}_m)]}{1 - f_v(\tilde{\varepsilon}_v - \tilde{\varepsilon}_m)q/[\tilde{\varepsilon}_m + q(\tilde{\varepsilon}_v - \tilde{\varepsilon}_m)]} \tag{2}$$

in which the thickness of individual layers and the tabulated dielectric constants of the metal and void domains were held constant while the void fraction, f_v, and depolarization factor, q, of the film nanostructure were allowed to vary (Figure 3a-b). The best fit for the series of data collected for an individual sample was obtained when the thickness of the CoP layer was selected as a constant value. A depolarization factor > 0.9 led to fits that were in close agreement with the measured data, and the predicted void fractions and thicknesses were consistent with AFM and SEM measurements of the films both before and after 10 min of activation.

Table 1: Comparison of optical properties of transparent metal films on planar semiconductors. The metal fraction, f_{metal}, and the depolarization factor, q, were modeled from ellipsometery data; measured and calculated transmittance, T_m and T_c, refer to the measured and calculated transmittance, respectively, under 700 nm illumination in an aqueous electrolyte.

Substrate	Material	Thickness	f_{metal}	q	T_m	T_c	Reference
InP	Rh	42 nm	0.49	0.45	0.65	0.35	(10)
InP	Pd	48 nm	0.32	0.32	0.67	0.47	(10)
InP	Re	60 nm	0.27	0.23	0.85	0.59	(10)
InP	Pt	33 nm	0.5	0.56	0.92[a)]	-	(9)
Si	CoP	42 nm	0.74	0.98	0.90	0.80	This work
Si	CoP	97 nm	0.78	0.93	-	0.24	This work
Si	CoP	125 nm	0.70	0.92	-	0.17	This work

a) Data were measured for a 633 nm source.

At a loading of 800 mC cm^{-2}, the void fraction increased asymptotically to 24 ± 2%, in close agreement with the 20 ± 2% fractional surface coverage of crevices measured by SEM (Figure S8-9). **Figure 3c-d** compares the simulated spectral transmittances described by a Maxwell-Garnett effective medium approximation as a function of thickness for two different nanostructured CoP films. Figure 3c is a close approximation of the CoP films studied in this work, with a host metal layer that includes a void fraction of 0.25 with a depolarization factor of 0.98. The transmittance fraction was roughly double the void fraction at a film thickness of 50 nm, and was larger than the void fraction for thicknesses up to 150 nm. Figure 3d presents the results obtained for discontinuous matrix of metallic spheres in a void ambient, represented by a characteristic depolarization factor of 0.33 and a metal fraction of 0.75. As q approaches 1, transmittances larger than values expected from a film composed of discontinuous catalyst particles are obtained. The case where $q = 1$ is consistent with a nanostructure having inclusions described by laminar, flat plates oriented normal to the direction of the electric field of incident

light, which is consistent with the observed film nanostructure in which flat mesas were separated by narrow, vertical sidewalls. **Table 1** compares the experimental and fitted optical parameters of films in this work with previously reported transparent metal catalysts films. CoP films in this work were represented by metal layers with disc-like void inclusions, in contrast to the void layers with spherical metal inclusions obtained for Pt, Pd, Rh, and Re; comparable or greater transmission coefficients were obtained for CoP films with increased metal loadings at an equivalent film thickness to that of the noble metal films.[21-22] Collectively, the measured and simulated transmittance spectra showed that the nanostructured CoP films transmitted more light than an equivalent fractional coverage of fully opaque, microscale metal islands, and demonstrate that films of a similar nanostructure with thicknesses in excess of 100 nm can overcome a linear tradeoff between increased mass loading of catalyst and decreased optical transmittance.

Table S1 compares the photoelectrochemical behavior of the devices investigated in this work to characteristics of other reported planar photocathodes for HER in strongly acidic electrolytes. Comparable values for $-J_{sc}$ have been reported for planar Si(100) surfaces coated with 5-7 nm of crystalline CoP,[35] 3.6 nm of MoS_2,[36] or 40-50 nm of MoS_xCl_y.[19] Stable photocurrents at negative potentials have been obtained for >100 h for devices which use MoS_2 and NiP_2 as catalysts, although such devices produced a current density of -10 mA cm^{-2} at more negative potentials than devices utilizing CoP, due to increased voltages required to drive the HER at these catalysts.[36-37] Electrodepositions of alloys containing Ni/NiP_x or Mo/MoS_x could hence be used to prepare transparent metal films that exhibit improved stability. Furthermore, the increased catalyst area obtained for thick, nanostructured films could reduce the voltage required to drive hydrogen evolution relative to thin, planar films.

The methods used to prepare transparent CoP films should be readily applicable to other electrodeposited metal phosphide films, containing Fe, Ni, Mo, or W.[38] Increasing the anisotropy of material removal, thereby increasing q, could lead to higher transmittances being obtained from such films. The insensitivity of the transmittance to film thickness, for film geometries in which the depolarization factor approaches unity, allows for higher mass loadings to be implemented in practice on the light-absorbing surface(s) of a photoelectrochemical device. Nanostructured metal phosphides could be prepared via activation in 0.50 M H_2SO_4(aq) and then implemented in device designed for operation in basic electrolyte. Metal phosphides have been reported as HER catalysts at pH > 13, although detailed characterization of crystalline Co_2P in 1.0 M KOH(aq) revealed a surface conversion of the phosphide to $Co(OH)_2$ after electrochemical cycling. Additionally, metal phosphides have been used as precursor species for efficient oxygen-evolution catalysts in 1.0 M KOH(aq) following conversion of the metal phosphide species to the corresponding metal oxide.[39-40]

Nanostructuring strategies that allow for increased mass loadings of catalyst to be utilized in photoelectrochemical devices could allow for the use of kinetically stable catalysts. Steady dissolution rates on the order of 0.4 pg s^{-1} cm^{-2} would be required to stabilize a 100 nm thick catalyst film for 10 years of operation, assuming that open-circuit corrosion cannot be eliminated (details on this calculation are provided in the supplemental information). Systematic studies of the corrosion of earth-abundant Co_2P, Ni_5P_4, and MoS_2 HER catalysts have revealed peak metal corrosion rates of ~1 ng s^{-1} cm^{-2} at open circuit in H_2(g)-saturated 0.10 M $HClO_4$(aq).[41] In this work, electrodeposited CoP in 0.50 M H_2SO_4(aq) under cathodic bias and following an initial substantial loss in Co exhibited corrosion rates comparable to those measured for crystalline Co_2P in 0.10 M $HClO_4$(aq).[41] The asymptotic corrosion rate of Co on n^+-Si(100)/Ti/CoP, along

with the gradual increase in the overpotential required to drive -10 mA cm^{-2} towards the HER, are consistent with previously reported chronoamperometric behavior for electrodeposited CoP films on metallic Cu.[29] These data are incompatible with failure mechanisms involving dissolution of catalyst or continued formation of interfacial SiO_x but delamination or passivation of the catalyst layer could be responsible for the decline in device performance.

In summary, optically transmissive films of an earth-abundant CoP HER catalyst were prepared for use in hydrogen-evolving photocathodes. Spontaneous generation of an open nanostructure occurred in minutes in 0.50 M H_2SO_4(aq) via anisotropic removal of acid-instable catalyst precursors along pre-existing boundaries. The process led to an increase in the weighted average optical transmissivity from 0.67 to 0.89 on FTO substrates, and resulted in a three-fold increase in the light-limited photocurrent density at a representative Si photocathode effecting the HER. The nanostructure adopted by these films is suitable for the increased catalyst loadings required for practical use of metal phosphides and the technique should be readily generalizable to other electrodeposited catalyst films that are deposited as a mixed composition of acid-stable and acid-instable species. Furthermore, this strategy could be used alone or in tandem with alternate light-management strategies to facilitate the use of earth-abundant catalysts on the light-incident side of a solar fuels device.

Experimental Methods

A detailed experimental section is provided in the supplemental information. Prior to the electrodeposition of Co, degenerately doped n-type Si(100) (n$^+$-Si) surfaces were metallized with 1 nm of Ti via RF sputtering to form an ohmic contact and adhesion layer for the CoP film. Metallized Si wafers and cleaned fluorine-doped tin-oxide samples were pre-nucleated with 2.5 nm of Co via RF sputtering. Electrodeposition was performed galvanostatically at a cathodic

current density of 20 mA cm^{-2} in a plating bath containing 0.20 M CoCl$_2$(aq) and 0.30 M

NaPO$_2$H$_2$(aq) continuously purged with Ar.[29] The thickness of the CoP film was controlled by

varying the deposition time. Films were activated via exposure to 0.50 M H$_2$SO$_4$(aq). The

effects of the acidic environment on the optical properties of the film were characterized in situ

under 1 atm of H$_2$(g) by transmission measurements during (photo)electrochemical hydrogen

evolution. The effects of activation on the film nanostructure were characterized ex situ by

scanning-electron microscopy (SEM), atomic-force microscopy (AFM), and spectroscopic

ellipsometry, after rinsing the films with deionized H$_2$O and drying in N$_2$(g).

Conflict of Interest: The authors have no conflicts of interest to declare.

Supporting Information: Supporting Information, including a detailed experiment experimental
section, additional AFM characterization, measurements of corrosion rates via ICP-MS,
extended chronoamperometry data, comparisons to photocathodes decorated with Pt, scanning
electron micrographs, complex index of refraction data for CoP and Co, additional ellipsometry
data for various film thicknesses, an estimation of corrosion rates in a solar fuels device, and
tabulated figures of merit for photocathodes utilizing earth abundant catalysts, is available.

References

1.   Heller, A., Hydrogen-evolving solar cells. *Science* **1984,** *223* (4641), 1141-1148.
2.   Bookbinder, D. C.; Bruce, J. A.; Dominey, R. N.; Lewis, N. S.; Wrighton, M. S.,
Synthesis and characterization of a photosensitive interface for hydrogen generation: Chemically
modified p-type semiconducting silicon photocathodes. *Proc. Natl. Acad. Sci.* **1980,** *77* (11),
6280-6284.
3.   Trotochaud, L.; Mills, T. J.; Boettcher, S. W., An optocatalytic model for semiconductor–
catalyst water-splitting photoelectrodes based on in situ optical measurements on operational
catalysts. *J. Phys. Chem. Lett.* **2013,** *4* (6), 931-935.
4.   Sun, K.; Moreno-Hernandez, I. A.; Schmidt, W. C.; Zhou, X.; Crompton, J. C.; Liu, R.;
Saadi, F. H.; Chen, Y.; Papadantonakis, K. M.; Lewis, N. S., A comparison of the chemical,

optical and electrocatalytic properties of water-oxidation catalysts for use in integrated solar-fuel generators. *Energy Environ. Sci.* **2017,** *10* (4), 987-1002.

5.　　Kibsgaard, J.; Tsai, C.; Chan, K.; Benck, J. D.; Nørskov, J. K.; Abild-Pedersen, F.; Jaramillo, T. F., Designing an improved transition metal phosphide catalyst for hydrogen evolution using experimental and theoretical trends. *Energy Environ. Sci.* **2015,** *8* (10), 3022-3029.

6.　　McCrory, C. C.; Jung, S.; Ferrer, I. M.; Chatman, S. M.; Peters, J. C.; Jaramillo, T. F., Benchmarking hydrogen evolving reaction and oxygen evolving reaction electrocatalysts for solar water splitting devices. *J. Am. Chem. Soc.* **2015,** *137* (13), 4347-4357.

7.　　Wang, H.-P.; Sun, K.; Noh, S. Y.; Kargar, A.; Tsai, M.-L.; Huang, M.-Y.; Wang, D.; He, J.-H., High-performance a-Si/c-Si heterojunction photoelectrodes for photoelectrochemical oxygen and hydrogen evolution. *Nano Lett.* **2015,** *15* (5), 2817-2824.

8.　　Tan, C. S.; Kemp, K. W.; Braun, M. R.; Meng, A. C.; Tan, W.; Chidsey, C. E.; Ma, W.; Moghadam, F.; McIntyre, P. C., > 10% solar-to-hydrogen efficiency unassisted water splitting on ALD-protected silicon heterojunction solar cells. *Sustainable Energy Fuels* **2019,** *3*, 1490-1500.

9.　　Bae, D.; Pedersen, T.; Seger, B.; Malizia, M.; Kuznetsov, A.; Hansen, O.; Chorkendorff, I.; Vesborg, P. C., Back-illuminated Si photocathode: a combined experimental and theoretical study for photocatalytic hydrogen evolution. *Energy Environ. Sci.* **2015,** *8* (2), 650-660.

10.　　Cabán-Acevedo, M.; Stone, M. L.; Schmidt, J. R.; Thomas, J. G.; Ding, Q.; Chang, H.-C.; Tsai, M.-L.; He, J.-H.; Jin, S., Efficient hydrogen evolution catalysis using ternary pyrite-type cobalt phosphosulphide. *Nat. Mat.* **2015,** *14*, 1245-1251.

11.　　Thalluri, S. M.; Wei, B.; Welter, K.; Thomas, R.; Smirnov, V.; Qiao, L.; Wang, Z.; Finger, F.; Liu, L., Inverted Pyramid textured P-Silicon Covered with Co2P as an Efficient and Stable Solar Hydrogen Evolution Photocathode. *ACS Energy Lett.* **2019,** *4* (7), 1755-1762.

12.　　Vijselaar, W.; Westerik, P.; Veerbeek, J.; Tiggelaar, R. M.; Berenschot, E.; Tas, N. R.; Gardeniers, H.; Huskens, J., Spatial decoupling of light absorption and catalytic activity of Ni–Mo-loaded high-aspect-ratio silicon microwire photocathodes. *Nat. Energy* **2018,** *3* (3), 185-192.

13.　　Kempler, P. A.; Gonzalez, M. A.; Papadantonakis, K. M.; Lewis, N. S., Hydrogen Evolution with Minimal Parasitic Light Absorption by Dense Co–P Catalyst Films on Structured p-Si Photocathodes. *ACS Energy Lett.* **2018,** *3* (3), 612-617.

14.　　Yalamanchili, S.; Kempler, P. A.; Papadantonakis, K. M.; Atwater, H. A.; Lewis, N. S., Integration of electrocatalysts with silicon microcone arrays for minimization of optical and overpotential losses during sunlight-driven hydrogen evolution. *Sustainable Energy Fuels* **2019,** *3*, 2227-2236.

15.　　Shaner, M. R.; McKone, J. R.; Gray, H. B.; Lewis, N. S., Functional integration of Ni–Mo electrocatalysts with Si microwire array photocathodes to simultaneously achieve high fill factors and light-limited photocurrent densities for solar-driven hydrogen evolution. *Energy Environ. Sci.* **2015,** *8* (10), 2977-2984.

16.　　Oh, S.; Song, H.; Oh, J., An optically and electrochemically decoupled monolithic photoelectrochemical cell for high-performance solar-driven water splitting. *Nano Lett.* **2017,** *17* (9), 5416-5422.

17.　　Chen, Y.; Sun, K.; Audesirk, H.; Xiang, C.; Lewis, N. S., A quantitative analysis of the efficiency of solar-driven water-splitting device designs based on tandem photoabsorbers patterned with islands of metallic electrocatalysts. *Energy Environ. Sci.* **2015,** *8*, 1736-1747.

18.   Zhang, H.; Ding, Q.; He, D.; Liu, H.; Liu, W.; Li, Z.; Yang, B.; Zhang, X.; Lei, L.; Jin, S., A p-Si/NiCoSex core/shell nanopillar array photocathode for enhanced photoelectrochemical hydrogen production. *Energy Environ. Sci.* **2016,** *9* (10), 3113-3119.

19.   Ding, Q.; Zhai, J.; Cabán-Acevedo, M.; Shearer, M. J.; Li, L.; Chang, H. C.; Tsai, M. L.; Ma, D.; Zhang, X.; Hamers, R. J., Designing Efficient Solar-Driven Hydrogen Evolution Photocathodes Using Semitransparent MoQxCly (Q= S, Se) Catalysts on Si Micropyramids. *Adv. Mater.* **2015,** *27* (41), 6511-6518.

20.   Ding, Q.; Song, B.; Xu, P.; Jin, S., Efficient electrocatalytic and photoelectrochemical hydrogen generation using MoS2 and related compounds. *Chem* **2016,** *1* (5), 699-726.

21.   Heller, A.; Aspnes, D.; Porter, J.; Sheng, T.; Vadimsky, R., Transparent Metals Preparation and Characterization of Light-Transmitting Platinum Films. *J. Phys. Chem.* **1985,** *89* (21), 4444-4452.

22.   Degani, Y.; Sheng, T.; Heller, A.; Aspnes, D.; Studna, A.; Porter, J., "Transparent" metals: preparation and characterization of light-transmitting palladium, rhodium, and rhenium films. *J. Electroanal. Chem.* **1987,** *228* (1-2), 167-178.

23.   Cheng, W.-H.; Richter, M. H.; May, M. M.; Ohlmann, J.; Lackner, D.; Dimroth, F.; Hannappel, T.; Atwater, H. A.; Lewerenz, H.-J., Monolithic photoelectrochemical device for direct water splitting with 19% efficiency. *ACS Energy Lett.* **2018,** *3* (8), 1795-1800.

24.   Heller, A.; Aharon-Shalom, E.; Bonner, W.; Miller, B., Hydrogen-Evolving Semiconductor Photocathodes: Nature of the Junction and Function of the Platinum Group Metal Catalyst. *J. Am. Chem. Soc.* **1982,** *104* (25), 6942-6948.

25.   Aspnes, D.; Heller, A.; Porter, J., Microstructurally engineered, optically transmissive, electrically conductive metal films. *J. Appl. Phys.* **1986,** *60* (9), 3028-3034.

26.   McEnaney, J. M.; Crompton, J. C.; Callejas, J. F.; Popczun, E. J.; Read, C. G.; Lewis, N. S.; Schaak, R. E., Electrocatalytic hydrogen evolution using amorphous tungsten phosphide nanoparticles. *Chem. Commun.* **2014,** *50* (75), 11026-11028.

27.   Popczun, E. J.; McKone, J. R.; Read, C. G.; Biacchi, A. J.; Wiltrout, A. M.; Lewis, N. S.; Schaak, R. E., Nanostructured nickel phosphide as an electrocatalyst for the hydrogen evolution reaction. *J. Am. Chem. Soc.* **2013,** *135* (25), 9267-9270.

28.   Popczun, E. J.; Read, C. G.; Roske, C. W.; Lewis, N. S.; Schaak, R. E., Highly active electrocatalysis of the hydrogen evolution reaction by cobalt phosphide nanoparticles. *Angew. Chem. Int. Ed.* **2014,** *53* (21), 5427-5430.

29.   Saadi, F. H.; Carim, A. I.; Verlage, E.; Hemminger, J. C.; Lewis, N. S.; Soriaga, M. P., CoP as an acid-stable active electrocatalyst for the hydrogen-evolution reaction: electrochemical synthesis, interfacial characterization and performance evaluation. *J. Phys. Chem. C* **2014,** *118* (50), 29294-29300.

30.   Saadi, F. H.; Carim, A. I.; Drisdell, W. S.; Gul, S.; Baricuatro, J. H.; Yano, J.; Soriaga, M. P.; Lewis, N. S., Operando spectroscopic analysis of CoP films electrocatalyzing the hydrogen-evolution reaction. *J. Am. Chem. Soc.* **2017,** *139* (37), 12927-12930.

31.   Stern, L.-A.; Liardet, L.; Mayer, M. T.; Morales-Guio, C. G.; Grätzel, M.; Hu, X., Photoelectrochemical deposition of CoP on cuprous oxide photocathodes for solar hydrogen production. *Electrochim. Acta* **2017,** *235*, 311-316.

32.   Aspnes, D. E., Optical properties of thin films. *Thin Solid Films* **1982,** *89* (3), 249-262.

33.   Palik, E. D., *Handbook of Optical Constants of Solids*. Academic press: 1998; Vol. 3.

34.   Sihvola, A. H.; Kong, J. A., Effective permittivity of dielectric mixtures. *IEEE Trans. Geosci. Remote Sens.* **1988,** *26* (4), 420-429.

35.   Hellstern, T. R.; Benck, J. D.; Kibsgaard, J.; Hahn, C.; Jaramillo, T. F., Engineering Cobalt Phosphide (CoP) Thin Film Catalysts for Enhanced Hydrogen Evolution Activity on Silicon Photocathodes. *Adv. Energy Mat.* **2016,** *6* (4).

36.   Benck, J. D.; Lee, S. C.; Fong, K. D.; Kibsgaard, J.; Sinclair, R.; Jaramillo, T. F., Designing active and stable silicon photocathodes for solar hydrogen production using molybdenum sulfide nanomaterials. *Adv. Energy Mat.* **2014,** *4* (18), 1400739.

37.   Hwang, S.; Porter, S. H.; Laursen, A. B.; Yang, H.; Li, M.; Manichev, V.; Calvinho, K. U.; Amarasinghe, V.; Greenblatt, M.; Garfunkel, E., Creating stable interfaces between reactive materials: titanium nitride protects photoabsorber–catalyst interface in water-splitting photocathodes. *J. Mat. Chem. A* **2019,** *7* (5), 2400-2411.

38.   Izhar, S.; Nagai, M., Transition metal phosphide catalysts for hydrogen oxidation reaction. *Catal. Today* **2009,** *146* (1-2), 172-176.

39.   Jin, S., Are Metal Chalcogenides, Nitrides, and Phosphides Oxygen Evolution Catalysts or Bifunctional Catalysts? *ACS Energy Lett.* **2017,** *2* (8), 1937-1938.

40.   Stern, L.-A.; Feng, L.; Song, F.; Hu, X., Ni 2 P as a Janus catalyst for water splitting: the oxygen evolution activity of Ni 2 P nanoparticles. *Energy Environ. Sci.* **2015,** *8* (8), 2347-2351.

41.   Ledendecker, M.; Mondschein, J. S.; Kasian, O.; Geiger, S.; Göhl, D.; Schalenbach, M.; Zeradjanin, A.; Cherevko, S.; Schaak, R. E.; Mayrhofer, K., Stability and Activity of Non-Noble-Metal-Based Catalysts Toward the Hydrogen Evolution Reaction. *Angew. Chem. Int. Ed.* **2017,** *56* (33), 9767-9771.